CHEMISTRY
A EUROPEAN JOURNAL

FULL PAPER

DOI: 10.1002/chem.201200970

Functionalization of Diameter Sorted Semi-conductive SWCNTs with Photosensitizing Porphyrins: Syntheses and Photoinduced Electron Transfer

Sushanta K. Das,[a] Atula S. D. Sandanayaka,[b] Navaneetha K. Subbaiyan,[a] Melvin E. Zandler,[c] Osamu Ito,*[d] and Francis D'Souza*[a, c]

Abstract: Covalent functionalization of diameter sorted SWCNTs with porphyrins (MP), and photochemistry to establish nanotube diameter-dependent charge separation efficiencies are reported. The MP–SWCNT(n,m) [M = 2H or Zn, and (n,m) = (7,6) or (6,5)] nanohybrids are characterized by a variety of spectroscopic, thermogravimetric, TEM imaging techniques, and also by DFT MO calculations. The thermogravimetric, Raman and fluorescence studies reveal the presence of a moderate number of porphyrins on the SWCNT surface. The MO results suggest charge separation (CS) via the excited state of MP. Time-resolved fluorescence studies reveal quenching of the singlet excited state of the MP with SWCNT(n,m), giving the rate constants of charge separation (k_{CS}) in the range of $(4–5)\times10^9\ s^{-1}$. Nanosecond transient absorption measurements confirm the charge-separated radical cation and the radical anion as [$MP^{\bullet+}$–$SWCNT^{\bullet-}$] with their characteristic absorption bands in the visible and near-IR regions. The charge separated states persist for about 70–100 ns thus giving an opportunity to utilize them to build photoelectrochemical cells, which allowed us to derive the structure–reactivity relationship between the nature of porphyrin and diameter of the employed nanotubes.

Keywords: charge separation · electron transfer · light-energy harvesting · photoelectrochemistry · porphyrins

Introduction

Single wall carbon nanotubes (SWCNTs)[1] are well known for their extraordinary mechanical, electronic and optical properties.[2] These SWCNTs with novel properties are predicted to be highly useful for a large number of innovative applications, especially when they are incorporated into new functional materials.[2,3] Among these applications, the most promising are in material science (ultralight and robust composite materials), in biology (imaging, sensing, biosensing and drug delivery systems), in electronics (transistors), and opto-electronics (photodetectors and photovoltaic devices).[4–9] Notably, the application of SWCNTs to energy conversion is fundamentally connected to the role as electron acceptors and/or electron donors. Consequently, carbon nanotube-based nanohybrids/conjugates with electron donors and acceptors have been the focus of several studies in recent years.[6–10] Such association with electron–donor or electron–acceptors is shown to modulate the electronic properties of SWCNTs.

The structures and properties of SWCNT relate to a pair of indices (n,m) referring to their diameter and chirality; that is, when n and m are different, SWCNTs are semiconducting, when n and m are a multiple of three, these are metallic.[2] To derive better structure–activity relations for the above-mentioned wide applications, it is essential to use sorted nanotubes according to their (n,m) indices, since the physicochemical properties, including optical absorption and emission,[11] redox properties and band gaps vary as a function of (n,m) indices of SWCNTs.[12] The bulk separation of nanotubes according to their (n,m) indices is still being developed; efforts to sort the HiPCO® nanotubes by using density gradient centrifugation and gel electrophoresis, and CoMoCAT® catalytic method of growing SWCNTs of narrow distribution of tube diameter by South West Nano Technologies are noteworthy accomplishments.[13–15]

Recently, by developing elegant self-assembled supramolecular approaches, we formed nanohybrids comprised of various electron–donor or electron–acceptor photosensitizers and diameter-sorted single-wall carbon nanotubes.[16,17]

[a] S. K. Das, Dr. N. K. Subbaiyan, Prof. F. D'Souza
Department of Chemistry, University of North Texas
1155 Union Circle, 305070, Denton, TX 76203-5017 (USA)
E-mail: Francis.DSouza@UNT.edu

[b] Dr. A. S. D. Sandanayaka
School of Materials Science
Japan Advanced Institute of Science and Technology (JAIST)
Nomi, Ishikawa, 923-1292 (Japan)

[c] Prof. M. E. Zandler, Prof. F. D'Souza
Department of Chemistry, Wichita State University
Wichita, KS 67260-0051 (USA)

[d] Prof. O. Ito
CarbonPhotoScience Laboratory, Kita-Nakayama 2-1-6
Izumi-ku, Sendai, 981-3215 (Japan)

Supporting information for this article is available on the WWW under http://dx.doi.org/10.1002/chem.201200970. These include The Raman spectra [pristine SWCNT(6,5) and H_2P–SWCNT(6,5)], TGA plots, TEM images [ZnP–SWCNT(n,m)], steady-state absorption spectra [UV/Vis/NIR for ZnP–SWCNT(n,m)], MO distribution and energy levels of ZnP–SWCNT(7,6), and nanosecond transient spectra of H_2P–SWCNT(n,m) in DMF.

By using these donor–acceptor nanohybrids, we were successful in demonstrating the effects of the nanometer diameter on photoinduced electron transfer leading to charge stabilization, photocatalytic electron pooling to accumulate redox products, and photoelectrochemical solar cells for direct conversion of light-into-electricity.[16,17]

However, to date, such investigations have not been performed on covalently functionalized SWCNT(*n*,*m*) with photosensitizer molecules, which will provide information on the effect of nanotube diameter on fine-tuned physicochemical properties. In the present study, we have accomplished this task by covalent functionalization of SWCNT-(7,6) and SWCNT(6,5) using a well-known photosensitizer electron donor: porphyrin.[18] In order to attach the porphyrins, we have employed Prato's method, that is, dipolar cycloaddition of azomethine ylide to produce pyrrolidine ring on the nanotube surface, as this method is mild enough to control the number of addends to a minimum number without significantly altering the electronic structure of the tubes.[19] The expected structures of these newly synthesized photoactive nanohybrids are shown in Scheme 1; a sufficient number of alkyl groups on the porphyrin periphery and ether chain on the pyrrolidine ring are introduced to increase the solubility. These nanohybrids have been characterized by using several optical, thermal, microscopic, and theoretical methods, and finally photoinduced electron transfer leading to charge separation and photoelectrochemical behavior has been systematically demonstrated. Furthermore, since each SWCNT(7,6) and SWCNT(6,5) with covalently connected porphyrin can be recognized as a dyad, the molecular orbital calculations were performed to visualize the frontier orbitals, from which an intramolecular charge-separation mechanism was elucidated.

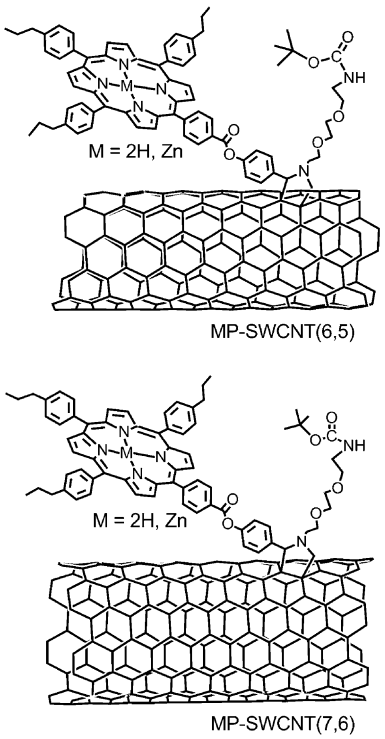

Scheme 1. Structures of MP–SWCNT(*n*,*m*) [M = 2H, Zn, and (*n*,*m*) = (6,5) and (7,6)] donor–acceptor nanohybrids synthesized by using Prato's method of dipolar cycloaddition of azomethine ylide.[19]

Results and Discussion

Synthesis of MP–SWCNT(*n*,*m*) donor–acceptor nanohybrids: Scheme 2 presents the multistep synthesis strategy adopted for the preparation of the MP–SWCNT nanohybrids; further details of the synthesis are given in the Experimental Section. Briefly, H_2-5(*p*-carboxyphenyl)-10,15,20-tri-(4-propyl)phenylporphyrin was synthesized by treating stoichiometric amounts of methyl-4-formylbenzoate, pyrrole and 4-propylbenzaldehyde in refluxing propionic acid followed by chromatographic separation. The methyl benzoate group was subjected to base hydrolysis to obtain H_2-5(*p*-carboxyphenyl)-10,15,20-tri(4-propyl)phenylporphyrin (**1**). The acid chloride form of porphyrin obtained by $SOCl_2$ treatment was reacted with hydroxybenzaldehyde followed by chromatographic separation to yield H_2-5-{4"-formyl-hydroxyphenyl-4′-phenylester}-10,15,20-tri(4-propyl)phenylporphyrin (**2**). In a separate experiment, *N*-[2-(*N*-Boc)2,2′-(ethylenedioxy)diethylamino]glycine (**3**) was synthesized (Scheme 2); Boc = $-C(=O)-O-C(CH_3)_3$. For the synthesis of H_2P–SWCNT (**4**), pristine SWCNT, **2** and **3** were refluxed in DMF at 120 °C for 24 h, yielding **4** as a black powder, which was dissolved in DMF, sonicated, centrifuged and filtered until all the unreacted components were washed away. Finally, H_2P–SWCNT(*n*,*m*) (**4**) was converted into ZnP–SWCNT(*n*,*m*) (**5**) by treatment with zinc acetate.

Raman and TEM imaging studies: Figure 1 shows the Raman spectra of pristine and H_2P–SWCNT(*n*,*m*) hybrids. The SWCNT(7,6) revealed a main band corresponding to the tangential mode (the graphitic G band) at 1584 cm^{-1},[2] whereas for H_2P–SWCNT(7,6), a weak band appeared at

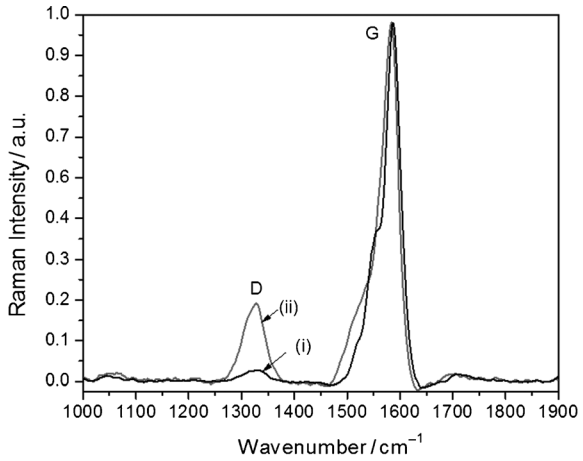

Figure 1. Raman spectra of: (i) pristine SWCNT(7,6), and (ii) dried sample of H_2P–SWCNT(7,6) excited by using a 532 nm laser light; both spectra are normalized to the G band position.

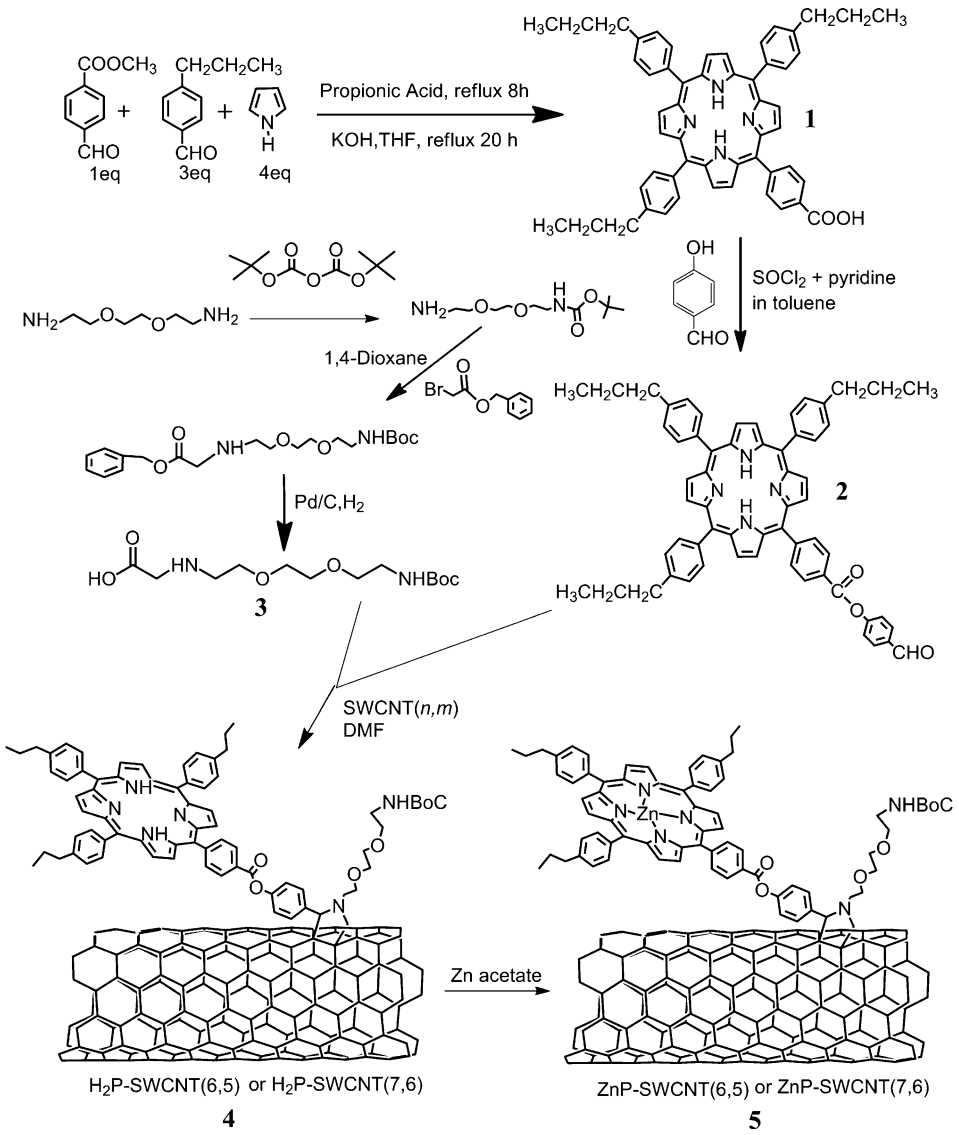

Scheme 2. Synthesis procedures for MP–SWCNT nanohybrids.

$1340\ cm^{-1}$, corresponding to the disorder mode (D band). Since the D band results from the chemical disruption of the sp^2 hybridized carbon atoms in the hexagonal framework of the nanotube walls,[20] the appearance of the D band is evidence for the covalent attachment of H_2P–pyrrolidine moiety onto the sidewalls of SWCNT(7,6). Similarly, an increase in the D band after functionalization of SWCNT(6,5) was observed compared to pristine SWCNT(6,5) (see Supporting Information Figure S1). The higher D band intensity observed for H_2P–SWCNT(7,6) indicates enhanced degree of functionalization compared to H_2P–SWCNT(6,5), a result that readily agrees with the thermogravimetric data discussed below.

The thermogravimetric analyses (TGA)[21] were performed on H_2P–SWCNT(*n*,*m*) hybrids; for the H_2P–SWCNT(6,5) hybrid, nearly 11% of the weight loss was observed in the 400–450 °C range corresponding to the organic fragments (see Supporting Information Figure S2 for TGA plots). For the H_2P–SWCNT-(7,6) hybrid, this weight loss was 17% at this temperature range. Using this information, for every 270 carbon atoms of SWCNT(6,5) one H_2P–pyrrolidine moiety was estimated, whereas for every 150 carbon atoms of SWCNT(7,6) one H_2P–pyrrolidine moiety was estimated. These results indicate higher chemical reactivity of the SWCNT(7,6) compared to the SWCNT(6,5).

Figure 2 shows the TEM images of the dry samples of pristine SWCNT(*n*,*m*) and H_2P–SWCNT(*n*,*m*). In the H_2P–SWCNT(*n*,*m*) hybrids, the SWCNT(*n*,*m*) bundles were found to be loosened by the covalent connection of H_2P, although some intertwining during sample preparation on the grid was observed. Similar TEM images were seen for ZnP–SWCNT(*n*,*m*) (see Supporting Information Figure S3). An apparent difference between MP–SWCNT(6,5) and MP–SWCNT(7,6) was not found in the TEM images. No significant nanocarbon particle or the catalyst impurities used in the synthesis of the tubes were observed, indicating higher purity upon functionalization of SWCNTs in the present study.

Absorption spectral studies: Figure 3 shows the optical absorption spectra of H_2P–SWCNT(*n*,*m*) in the UV/Vis/NIR regions in DMF. The absorption bands of the SWCNT(*n*,*m*) moieties appear in the NIR and visible regions; a main band at 1022 nm and a weak one at 583 nm for SWCNT(6,5), and a main band at 1170 nm and a weak one 667 nm for SWCNT(7,6), whereas the sharp absorption bands of the H_2P moieties appear in the UV/Vis regions (main band in the 415–420 nm region and weak bands in the 500–550 nm region; the 300 nm band may be due to the MP moieties). The absorption bands of SWCNT(*n*,*m*) in the nanohybrids were red-shifted by about $400\ cm^{-1}$ from that of the pristine SWCNT(*n*,*m*) peaks, due to the interaction with the π electrons of the H_2P moiety and chemical functionalization.[22,23] From the longest absorption sharp peaks, the band gaps can be evaluated to be 1.21 and 1.05 eV for SWCNT(6,5) and SWCNT(7,6), respectively, which show narrowing of 0.06–

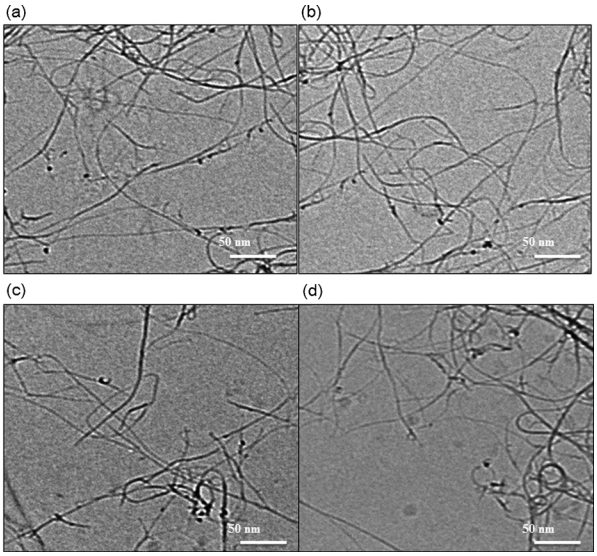

Figure 2. TEM images of: a) SWCNT(6,5), b) SWCNT(7,6), c) H_2P–SWCNT(6,5), and d) H_2P–SWCNT(7,6); scale bars 50 nm.

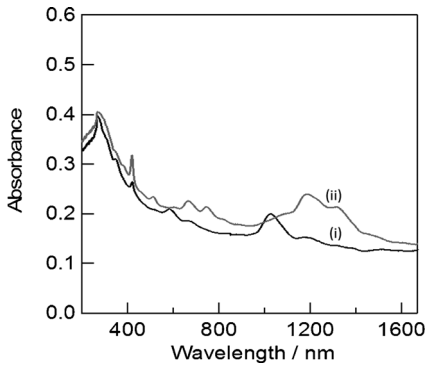

Figure 3. Steady-state absorption spectra of H_2P–SWCNT(*n*,*m*) in DMF with: (i) SWCNT(6,5), and (ii) SWCNT(7,6).

0.08 eV, due to chemical functionalization. Quite similar absorption spectra were observed for ZnP–SWCNT(*n*,*m*), in which the ZnP moiety showed a main band at 420–425 nm and weak bands in the 500–550 nm region (see Supporting Information Figure S4).

From the absorbance of about 0.1 of the MP-main band, the concentrations of ZnP and H_2P were evaluated to be $(1–3)\times10^{-7}$ mol on 0.1 mg of SWCNT(*n*,*m*), which corresponds to one MP in every 150–250 carbons of SWCNT, which are in good agreement with the result from TGA data. Compared with the reported noncovalent MP–SWCNT(*n*,*m*) hybrids,[16,17,24,25] the NIR absorption peaks in Figure 3 for the covalently bonded MP–SWCNT(*n*,*m*) are broader and weaker, suggesting that the covalent bonding disturbs the π-electron systems of the pristine SWCNT(*n*,*m*) to some extent.[19]

Structure optimization by DFT calculations: In order to visualize the geometry of the covalently linked porphyrin–nanotube hybrids, DFT energy optimization was performed by using the B3LYP/3-21G(*) basis set[26] on these computationally challenging systems. In these calculations, 318 carbons for SWCNT(6,5) and 268 carbons for SWCNT(7,6) in building the nanotube with one porphyrin unit were used for better understanding of the donor–acceptor hybrid electronic structure. Hydrogen atoms were bonded to the terminal carbons of the open tubes. Figure 4 shows the optimized

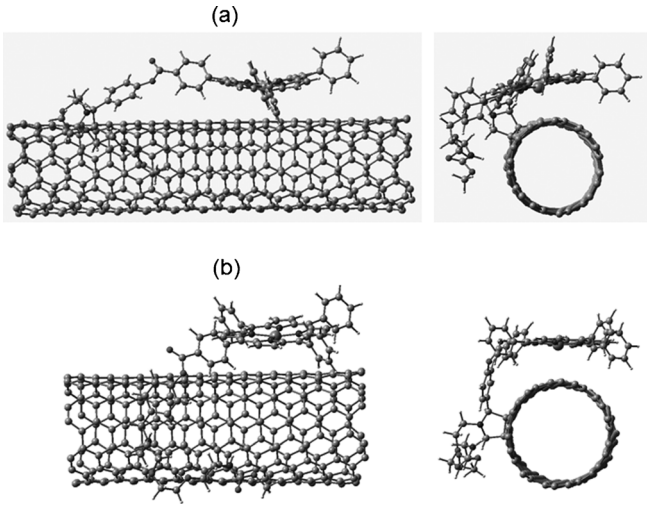

Figure 4. B3LYP/3-21G(*) optimized structure of: a) ZnP–SWCNT(6,5), in which a connected bond is seen at the upper surface, and b) ZnP–SWCNT(7,6), in which a connected bond is seen on the lower middle. Two views are shown for better visualization.

structures of the ZnP–SWCNT(6,5) and ZnP–SWCNT(7,6) hybrids in two views, in which a pyrrolidine ring is bonded to a C=C bond on SWCNT(*n*,*m*), converting to C−C bonds. The calculated diameter and length were 7.55 and 34.32 nm for SWCNT(6,5), and 8.98 and 24.48 nm for SWCNT(7,6), respectively; the diameters are in good agreement with the earlier reported STM and AFM images.[14] In both structures, close association of the ZnP to the surface of the SWCNT was predicted, which is possible from the bent ester bond connecting MP moiety and the pyrrolidine ring. The distance between the Zn atom to the closest carbon of SWCNT was found to be approximately 3.4 Å for both optimized structures. The alkoxy chain of the pyrrolidine ring was also close to the nanotube surface revealing some interactions. As shown in the edge-on-view of the hybrids on the right-hand side of each Figure, the ZnP positioning on the SWCNT surface was symmetric and almost flat in the case of ZnP–SWCNT(7,6), whereas for ZnP–SWCNT(6,5) the ZnP was slightly off and bent due to the smaller diameter of SWCNT(6,5). Although these optimized structures are calculated in "vacuum", they provide fairly good visualization of the donor–acceptor structures in solution, in which slightly different structures and interactions would be anticipated.

Energy level diagram: The MO energy levels were also calculated by the DFT calculations by using the optimized

structures in Figure 4. Some of the representative HOMO−n and LUMO+n (n=0, 1, 2, …) of ZnP–SWCNT-(6,5) are shown in Figure 5. HOMO and HOMO−1 have the electron density mainly on SWCNT(6,5), corresponding to the valence band of SWCNT(6,5). The electron distributions of HOMO and HOMO−1 are higher on the middle part of SWCNT(6,5) just under the ZnP compared with both sides; in addition, some electron distributions are also found on the ZnP moiety, suggesting occurrence of weak charge-transfer interactions in the ground state. On the other hand, HOMO−2 has the electron density predominantly localized on the ZnP moiety, corresponding to the local HOMO of the ZnP moiety, whereas HOMO−3 has the electron density localized on SWCNT(6,5) again. LUMO and LUMO+1 have the electron density localized on the whole SWCNT(6,5), corresponding to the conduction band of SWCNT(6,5). These LUMOs are also typical for LUMO+n ($\leq$10), although the ranges of the distributions vary with n, as shown for the LUMO+2 as an example, in which the electron densities gather under ZnP. At higher LUMOs the electron density was localized on the ZnP moiety corresponding to the local LUMO of the ZnP moiety, although n=10 is not an exact number due to the delocalization both to ZnP and SWCNT(6,5).

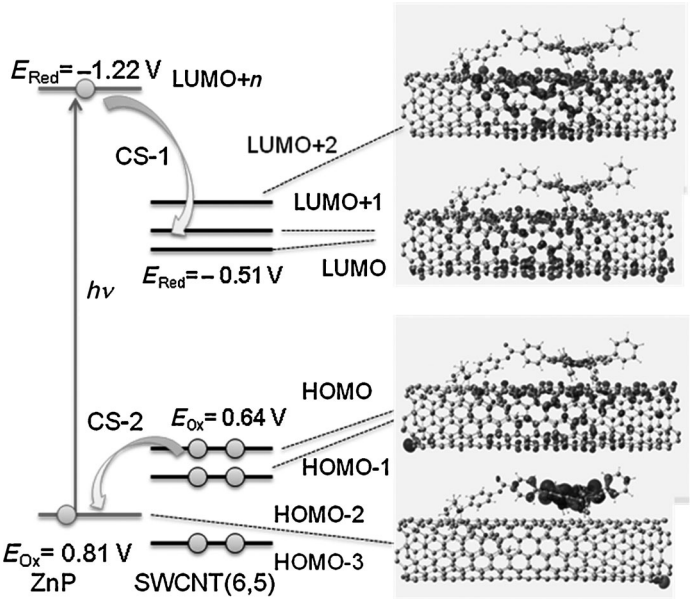

Figure 5. Energy diagrams with MOs of ZnP–SWCNT(6,5) for photoinduced charge separation. Left: MO energy levels of the ZnP moiety ($n\geq$10); center: MO energy levels of the SWCNT(6,5) moiety; right: the electron distributions of some representative MOs. The E_{Ox} and E_{Red} values of ZnP and SWCNT(6,5) versus Ag/AgCl.

The energy diagram in Figure 5 was constructed on combination of these MO energy levels and the observed redox potentials for the components, since the calculated values for such huge and distorted carbon π-electron systems are quite qualitative. Therefore, the reported oxidation potential of ZnP[27] corresponding to HOMO−2 and the redox potentials of SWCNTs in DMF[12] corresponding to the LUMO and HOMO, respectively, are added to the energy level diagram in Figure 5. By photoexcitation of the ZnP moiety, an electron from the HOMO−3 level is elevated to the LUMO+10 level within the ZnP moiety; thus, the reduction potential of ZnP is evaluated from the excitation energy (2.03 eV) from HOMO−2. From the excited state of the ZnP moiety (LUMO+10), the electron can transfer to the LUMO on SWCNT(6,5); thus, $MP^{\bullet+}$–$SWCNT^{\bullet-}$ can be formed, which is denoted as charge-separation process-1 (CS-1) in Figure 5. Similar MO distributions and energy levels were calculated for ZnP–SWCNT(7,6); some of them are shown in the Supporting Information (Figure S5).

The energy of $MP^{\bullet+}$–$SWCNT^{\bullet-}$ can be evaluated from the difference of the LUMO energy [E_{Red} of SWCNT(n,m)] and the HOMO energy (E_{Ox} of MP). Then, the free energy of the charge separation[28] ($\Delta G_{CS\text{-}1}$) from the lowest excited singlet state (^{1}ZnP*) can be evaluated to be −0.71 and −0.72 eV for SWCNT(6,5) and SWCNT(7,6), respectively. Similarly, $\Delta G_{CS\text{-}1}$ values for H_2P–SWCNT via ^1H_2P* (1.81 eV) can be evaluated to be −0.52 and −0.50 eV for SWCNT(6,5) and SWCNT(7,6), respectively [see Supporting Information Figure S5 for energy diagram with MO of ZnP–SWCNT(7,6)].

From the energy level diagram in Figure 5, the other CS process from the HOMO levels of SWCNT(n,m) to the half-vacant HOMO of ^{1}MP* generated after the photoexcitation is also possible, denoted as the CS-2 process, and gives $MP^{\bullet-}$–$SWCNT^{\bullet+}$. The free-energies for this process ($\Delta G_{CS\text{-}2}$) were estimated to be −0.17–−0.31 eV via ^{1}ZnP* and 0.04–−0.11 eV via ^1H_2P* for SWCNT(6,5) and SWCNT-(7,6), respectively. Considering lower exothermicity of CS-2 processes, CS-1 may be the predominant route for the occurrence of photoinduced electron transfer. From the energy diagram, sequential occurrence of CS-1 and CS-2 results in energy transfer; however, the widely distributed electron and hole along the SWCNTs may retain the CS states for a period.

Fluorescence measurements: Photochemistry and photophysical events via the excited state of the MP moiety of the covalently linked MP–SWCNT(n,m) (M=Zn and H_2) were probed by fluorescence measurements. Figure 6a shows the steady-state fluorescence spectra and the time-profiles of the fluorescence intensity of the H_2P–SWCNT(n,m) and ZnP–SWCNT(n,m) hybrids in DMF by the predominant excitation of the porphyrin moiety. H_2P samples exhibited a main fluorescence peak at 650 nm with an additional one at 720 nm. In the hybrids with SWCNT, the H_2P fluorescence intensities [H_2P–SWCNT(6,5), curve (i); H_2P–SWCNT(7,6), curve (ii)] were found to be quenched over 30% of its original intensity (data not shown), suggesting occurrence of some events via the ^1H_2P* state.[29] Similarly, ZnP–SWCNT(n,m) showed sharper peaks at 620 and 660 nm characteristic of ZnP fluorescence (Figure 6b). In the hybrids with SWCNT, the ZnP fluorescence intensity was found to be quenched over 40% of its original intensity

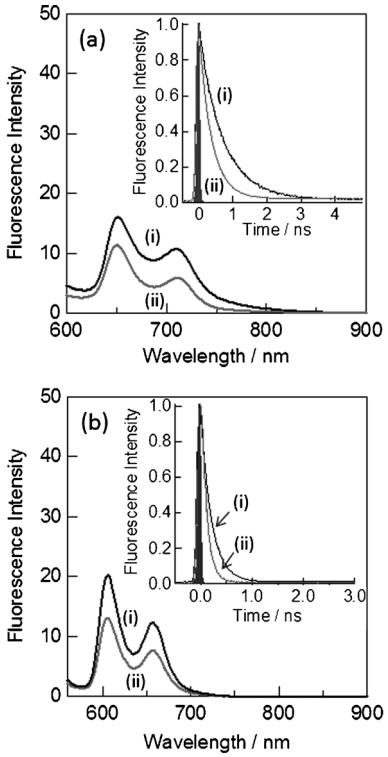

Figure 6. Steady-state fluorescence of MP–SWCNT(n,m) in DMF; $\lambda_{ex}=$ 550 nm, where the absorbance of the MP moiety is normalized for these solutions. Inset: fluorescence decay time profiles; $\lambda_{ex}=408$ nm. a) H_2P–SWCNT(n,m) (650–720 nm), and b) ZnP–SWCNT(n,m) (600–680 nm). (i) SWCNT(6,5), and (ii) SWCNT(7,6).

(data not shown), suggesting occurrence of events via ^{1}ZnP*.

The fluorescence quenching for MP–SWCNT(7,6) was found to be more efficient than that of MP–SWCNT(6,5). It must be noted here that the steady-state quenching experiments of the MP–SWCNT(n,m) are quite qualitative, because some broad absorptions of the SWCNT(n,m) overlap with the MP absorption in the visible region, making it difficult to normalize the MP excitation intensity. Therefore, it is essential to measure the fluorescence time profiles (see insets in Figure 6 and analyses in the following paragraphs), which are independent of MP concentration in a relatively wide range.

As for photophysical events via the ^{1}MP* state in polar solvents, such as DMF, electron transfer may be more favorable than energy transfer.[30] In order to check the occurrence of energy transfer from ^{1}MP* to SWCNT(n,m), the NIR emission of the SWCNT(n,m) was monitored by the excitation of the MP moieties in MP–SWCNT(n,m). No increase in the emission intensity from SWCNT(n,m) in the NIR region upon MP excitation was observed in DMF, eliminating energy transfer as one of the quenching mechanisms. Hence, in polar DMF, electron transfer (charge separation) via ^{1}MP* in MP–SWCNT(n,m) is considered as a main origin of fluorescence quenching, which is supported by the evaluated negative ΔG_{CS} values.

From the picosecond fluorescence time-profile measurements with the streak-scope method (insets in Figure 6), it can be seen that the presence of SWCNT(6,5) and SWCNT-(7,6) in the hybrids accelerated the ZnP and H_2P fluorescence decays. By curve-fitting the time profiles with a bi-exponential decay function, the MP-fluorescence lifetimes [$(\tau_f)_{hybrid}$] were evaluated to be 80–330 ps with major fractions (F) of 82–92% (Table 1). The minor fractions may be attributed to no-interacting MPs, because their lifetimes are similar to those of the pristine MPs. From the short $(\tau_f)_{hybrid}$ values, the rate constant and quantum yield for the MP fluorescence quenching can be calculated; on combining the above considerations, these values can be attributed to charge separation rate constant (k_{CS}) and quantum yield (Φ_{CS}), which are listed in Table 1.

Table 1. Observed fluorescence lifetimes [$(\tau_f)_{hybrid}$] and estimated rate parameters (k_{CS} and Φ_{CS}) for charge separation of MP–SWCNT(n,m) hybrids in DMF.[a]

MP–SWCNT(n,m)	$(\tau_f)_{hybrid}$ [ps] (F [%])	k_{CS}[a] [s^{-1}]	Φ_{CS} ($\times F$)
ZnP–SWCNT(6,5)	110 (89)	9.5×10^9	0.99 (0.88)
ZnP–SWCNT(7,6)	80 (92)	12.0×10^9	0.99 (0.92)
H_2P–SWCNT(6,5)	330 (82)	2.5×10^9	0.84 (0.68)
H_2P–SWCNT(7,6)	220 (90)	4.2×10^9	0.89 (0.80)

[a] $k_{CS}=(1/\tau_f)_{hybrid}-(1/\tau_f)_{ref}$; $\Phi_{CS}=[(1/\tau_f)_{hybrid}-(1/\tau_f)_{ref}]/(1/\tau_f)_{hybrid}$; $(\tau_f)_{ref}=$ 1450 ps for ZnP and 2000 ps for H_2P in DMF.

The evaluated k_{CS} and Φ_{CS} for ZnP–SWCNT(n,m) in DMF were found to be in the ranges of $(9.5–12.0)\times10^9$ s^{-1} and 0.88–0.92 (including interacting fraction), which are larger than those of H_2P–SWCNT(n,m) in the rage of $(2.5–4.2)\times10^9$ s^{-1} for k_{CS} and 0.68–0.80 for Φ_{CS}. This trend is in agreement with the exothermic trends in both the CS-1 and CS-2 processes evaluated from both $\Delta G_{CS\text{-}1}$ and $\Delta G_{CS\text{-}2}$, which are mainly determined by small E_{Ox}. The values of k_{CS} and Φ_{CS} for MP–SWCNT(7,6) are slightly larger than those for MP–SWCNT(6,5), suggesting that SWCNT(7,6) with the higher conduction band level is more favorable for charge separation via ^{1}MP* compared with SWCNT(6,5) with the lower conduction band level.

Nanosecond transient absorption studies: Evidence for charge separation and the rate constant of charge recombination, k_{CR}, were obtained from transient absorption spectral studies by using a 532 nm laser light to excite the ZnP and H_2P moieties predominantly. Figure 7 shows the nanosecond transient absorption spectra of ZnP–SWCNT(n,m) nanohybrids in Ar-saturated DMF. Noticeably, a main transient absorption peak was observed at 620–650 nm, which can be attributed to the formation of ZnP$^{\bullet+}$.[16] In the NIR region, the broad absorption bands were observed, which can be ascribed to SWCNT(n,m)$^{\bullet-}$, as a partner of the ZnP$^{\bullet+}$ moiety, since both the band intensities decrease at the same rates. Indeed, the NIR band observed for SWCNT(6,5) (Figure 7a) is slightly sharper than that of SWCNT(7,6) (Figure 7b), suggesting these NIR bands are characteristic of

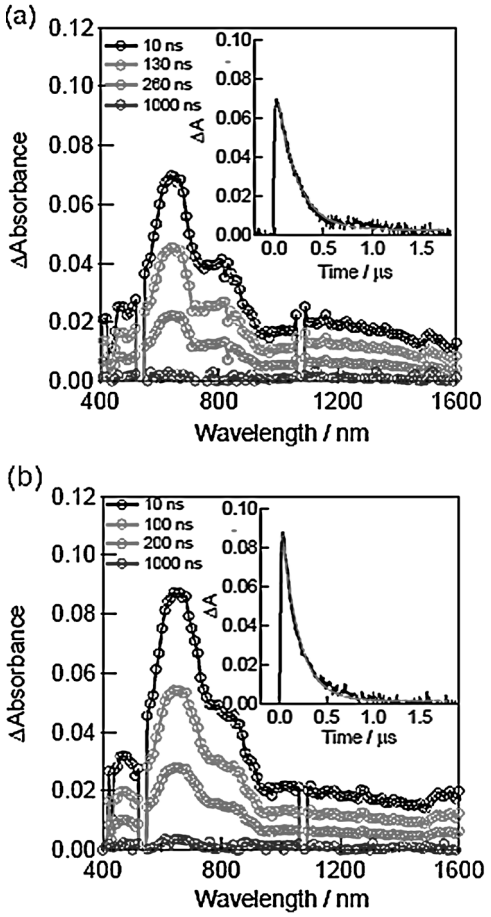

Figure 7. Nanosecond transient absorption spectra of ZnP–SWCNT(*n*,*m*) observed by 532 nm (ca. 3 mJ per pulse) laser irradiation in Ar-saturated DMF. Inset: absorption–time profile at 650 nm. a) ZnP–SWCNT(6,5), and b) ZnP–SWCNT(7,6). Spikes at 542 and 1064 nm are scattered light from SHG and fundamental of YAG laser.

SWCNT(6,5) and SWCNT(7,6). Similarly, H_2P–SWCNT(*n*,*m*) nanohybrids showed transient absorption spectra (see Supporting Information Figure S6) in which two broad absorption bands appear in the visible region (at 500 and 600–700 nm) and also in the NIR region. Although they are broader, the former VIS bands support the assignments to $H_2P^{\bullet+}$, and the latter NIR bands to SWCNT(*n*,*m*)$^{\bullet-}$.

From these broad transient bands, it was difficult to separately recognize two kinds of radical-ion pairs (RIPs), such as MP$^{\bullet+}$–SWCNT$^{\bullet-}$ and MP$^{\bullet-}$–SWCNT$^{\bullet+}$. Compared with the non-covalent MP–SWCNT(*n*,*m*) hybrids in our previous reports,[16,17] these transient spectra of the covalently bonded MP$^{\bullet-}$–SWCNT(*n*,*m*)$^{\bullet+}$ do not exhibit any distinct maxima; it can be noted here that the covalent bonding on SWCNT(*n*,*m*) considerably disturbs the π-electronic structures of the SWCNT(*n*,*m*).

The time profiles of ZnP$^{\bullet+}$ at 650 nm are shown in the insets of Figure 7. The increases in ZnP$^{\bullet+}$ are fast within the nanosecond laser pulse (6 ns); such quick rises correspond to the fast charge separation within about 100 ps as estimated from the ZnP fluorescence lifetimes. The decays of the ZnP$^{\bullet+}$ mostly persists until about 500 ns; from the first-order fitting to the decay curves until about 500 ns, the k_{CR} values were evaluated to be $(5–6)\times10^6\ s^{-1}$ (Table 2).

Table 2. Estimated rate parameters for charge recombination in DMF.[a]

Nanohybrids	k_{CR}[a] [s^{-1}]	τ_{RIP} [ns]	k_{CS}/k_{CR}[a]
ZnP–SWCNT(6,5)	4.9×10^6	210	1950
ZnP–SWCNT(7,6)	5.8×10^6	170	2070
H_2P–SWCNT(6,5)	6.4×10^6	160	390
H_2P–SWCNT(7,6)	7.5×10^6	130	550

[a] $k_{CS}=(1/\tau_f)_{hybrid}-(1/\tau_f)_{ref}$; $\Phi_{CS}=[(1/\tau_f)_{hybrid}-(1/\tau_f)_{ref}]/(1/\tau_f)_{hybrid}$; $(\tau_f)_{ref}$ = 1450 ps for ZnP and 2000 ps for H_2P in DMF.

From these k_{CR} values, the lifetimes of ZnP$^{\bullet+}$–SWCNT(*n*,*m*)$^{\bullet-}$, τ_{RIP} ($=1/k_{CR}$), were evaluated to be 170–210 ns. Similarly, the k_{CR} and τ_{RIP} values for $H_2P^{\bullet+}$–SWCNT(*n*,*m*)$^{\bullet-}$ were $(6–7)\times10^6\ s^{-1}$ and 130–160 ns, respectively (Table 2), indicating that ZnP$^{\bullet+}$–SWCNT$^{\bullet-}$ (or ZnP$^{\bullet-}$–SWCNT$^{\bullet+}$) persist for longer time than $H_2P^{\bullet+}$–SWCNT$^{\bullet-}$ (or $H_2P^{\bullet-}$–SWCNT$^{\bullet+}$) in DMF. The k_{CS}/k_{CR} ratios, which are widely used as the extent of "charge stabilization"[10] in photosynthetic systems and nanohybrids, were found to be 2000–2100 for ZnP–SWCNT(*n*,*m*), which are larger than those of H_2P–SWCNT(*n*,*m*) (390–550), suggesting higher charge stabilization of ZnP$^{\bullet+}$–SWCNT$^{\bullet-}$ (or ZnP$^{\bullet-}$–SWCNT$^{\bullet+}$). In both cases, SWCNT(7,6) had slightly larger k_{CS}/k_{CR} values than SWCNT(6,5), indicating that the best pair as the photoinduced charge-separation system was ZnP–SWCNT(7,6) in DMF.

Photoelectrochemical studies: The photoinduced charge-separation rates and stabilization observed in the investigated MP–SWCNT(*n*,*m*) impelled us to perform photoelectrochemical studies[31] to visualize their ability to convert light energy into electricity. To this aim, the MP–SWCNT(*n*,*m*) nanohybrids in DMF solution were drop-coated on nanoclustered SnO_2/FTO electrode surface (FTO; fluorine doped tin oxide), in which FTO/SnO_2 was selected due to its E_{Red} as low as those of SWCNT(*n*,*m*). The photocurrent action spectra based on incident photon conversion efficiency (IPCE %)[32] values in the wavelength region covering up to 700 nm show a peak near 420–440 nm (Figure 8) corresponding to the absorption of the MP moieties, although the overall IPCE % values were low, which could be due to a lower number of porphyrin entities and quenching of porphyrin emission in the donor–acceptor hybrids. Among the earlier reported nanohybrids assembled with the porphyrin derivatives by some supramolecular approaches,[16] the present IPCEs look to be moderate. The photoswitching responses shown in the inset of Figure 8 revealed quick response and light stability of these nanohybrids. The maximal IPCE values follow the trends of k_{CS}/k_{CR} in Table 2, suggesting that the photovoltaic cell efficiency strongly depends upon the charge separation stability. Consequently, higher values for SWCNT(7,6) compared to SWCNT(6,5) derived

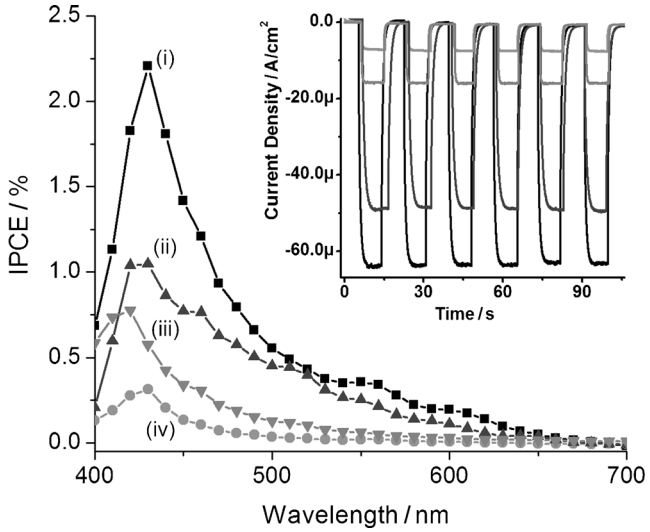

Figure 8. IPCE spectra and (inset) light-current switching curves for the photoelectrochemical cells of: (i) ZnP–SWCNT(7,6), (ii) ZnP–SWCNT-(6,5), (iii) H_2P–SWCNT(7,6), and (iv) H_2P–SWCNT(6,5) coated on SnO_2-modified FTO electrode surface in acetonitrile containing LiI (0.5 M) and I_2 (0.1 M) mediator.

nanohybrids, and higher values for ZnP over H_2P derived nanohybrids were observed.

Conclusion

Light energy harvesting donor–acceptor nanohybrids comprised of porphyrins and diameter-sorted SWCNT(*n*,*m*) were newly synthesized and characterized. In order to connect the porphyrins (MP) covalently to the side walls of SWCNT(*n*,*m*), Prato's method of dipolar cycloaddition of azomethine ylide was employed, which largely preserved the π electronic structure of SWCNT(*n*,*m*) after functionalization, which were evident from the TGA and Raman studies. The theoretical DFT-MO calculations of the MP–SWCNT-(*n*,*m*) nanohybrids provided the optimized structures and the MO energy levels; on combining the redox values, possible mechanisms of electron transfer and the free-energy calculations were estimated. The steady-state and time-resolved fluorescence studies revealed efficient quenching of the singlet excited states of the ZnP and H_2P moieties; the nanosecond transient absorption technique confirmed an electron transfer process, producing $MP^{\bullet+}$–$SWCNT^{\bullet-}$ (or $MP^{\bullet-}$–$SWCNT^{\bullet+}$) charge separation species. The merit of charge-separated state stabilization, which were calculated from the rates of charge separation, k_{CS} and rate of charge recombination, k_{CR} were found to be higher for ZnP than H_2P and slightly higher for the MP–SWCNT(7,6) than MP–SWCNT(6,5) hybrids. As a proof-of-concept, photoelectrochemical solar cells built by using these MP–SWCNT(*n*,*m*) on the modified FTO/SnO_2 electrodes gave best performance for ZnP–SWCNT(7,6) as predicted from the merit of charge-separated state stabilization evaluated by time-resolved spectral data.

Experimental Section

Chemicals: The (6,5 and 7,6) enriched SWCNTs were from CoMoCAT®, SourthWest Nano Technologies, Inc., (Norman, OK)[15] marketed by Aldrich Chemicals (Milwaukee, WI). The bulk solvents utilized in the spectral and photophysical measurements were from Aldrich.

Synthesis of MP–SWCNT(*n*,*m*) donor–acceptor hybrids

H_2-5(*p*-methoxycarbonylphenyl)-10,15,20-tri(4-propyl)phenyl porphyrin (1a): This compound was synthesized according to Adler et al.[33] A mixture of methyl-4-formylbenzoate (1.2 g, 7.3 mmol), pyrrole (1.99 mL, 29.2 mmol) and 4-propylbenzaldehyde (3.23 mL, 21.9 mmol) was refluxed in propionic acid (200 mL) for 8 h. The propionic acid was removed under reduced pressure and the crude product was purified on basic alumina column by using hexane: CH_2Cl_2 (1:1 v/v). Yield: 1.38 g, 25%; ^{1}H NMR ($CHCl_3$-d): δ = 8.9–8.75 (m, 8H, β-pyrrolic *H*), 8.45 (d, 2H, phenyl H), 8.3 (d, 2H, phenyl H), 8.14–8.06 (m, 6H, *o*-phenyl H), 7.53–7.58 (m, 6H, *m*-phenyl H), 4.3 (s, 3H, methoxy H), 2.9 (t, 6H, propyl $-CH_2$H), 1.9 (sextet, 6H, propyl-CH_2H), 1.18 (t,9H, propyl-CH_3H), −2.78 ppm (s, br, 2H, imino H); ESI mass in $CHCl_3$ calcd for $C_{55}H_{50}N_4O_2$, 799.01; found: *m*/*z* (%): 799.6 [M^+] (100), 800.5 [M^+] (60), 801.5 [M^+] (15).

H_2-5(*p*-carboxyphenyl)-10,15,20-tri(4-propyl)phenylporphyrin (1): A mixture of **1a** (200 mg, 0.25 mmol) in THF (20 mL) and excess of KOH (5 g, saturated solution in water) was refluxed for 20 h. After being cooled, the mixture was diluted with CH_2Cl_2, acidified with conc. HCl and extracted. The organic layer was washed with saturated $NaHCO_3$ solution and dried over anhydrous Na_2SO_4. Solvent was evaporated and the crude product was purified on silica gel column by using $CHCl_3$/CH_3OH (95:5 v/v). Yield: 0.158 g, 80%; ^{1}H NMR ($CHCl_3$-d): δ = 8.94–8.78 (m, 8H, β-pyrrolic *H*), 8.6 (d, 2H, phenyl H), 8.3 (d, 2H, phenyl H), 8.18–8.08 (m, *o*-phenyl H), 7.6–7.53 (m, 6H, *m*-phenyl H), 2.9 (t, 6H, propyl-CH_2H), 1.9 (sextet, 6H, propyl-CH_2H), 1.18 (t, 9H, propyl-CH_3H), −2.78 ppm (s, br, 2H, −NH); ESI mass in $CHCl_3$ calcd for $C_{54}H_{48}N_4O_2$, 784.98; found: *m*/*z* (%): 785.5 [M^+] (100), 786.5 [M^+] (62), 787.5 [M^+] (17).

H_2-5-{4"formylhydroxyphenyl-4′-phenylester}-10,15,20-tri(4-propyl)phenylporphyrin (2): A solution of **1** (150 mg, 0.19 mmol), $SOCl_2$ (150 μL, 1.9 mmol) and pyridine (1 mL) in dry toluene (40 mL) was refluxed under argon for 3 h. After being cooled, the solvent was evaporated and the resultant mixture was redissolved in dry toluene (40 mL). Then pyridine (1 mL) was added followed by 4-hydroxybenzaldehyde (46 mg, 0.38 mmol). Reaction mixture was stirred at room temperature under argon for 12 h. Solvent was evaporated and the crude compound was purified by column chromatography on silica gel by using hexane/CH_2Cl_2 (10:90 v/v). Yield: 0.118 g, 70%; ^{1}H NMR ($CHCl_3$-d): δ = 10.1 (s, 1H, −CHO H), 8.94–8.8 (m, 8H, β-pyrrolic H), 8.6 (d, 2H, phenyl H), 8.4 (d,2H, phenyl H), 8.14–8.10 (m, *o*-phenyl H), 8.08 (d, 2H, phenyl H), 7.6 (d, 2H, phenyl H), 7.52–7.58 (m, 6H, *m*-phenyl H), 2.9 (t, 6H, propyl-CH_2H), 1.9 (sextet, 6H, propyl-CH_2H), 1.18 (t, 9H, propyl-CH_3H), −2.78 ppm (s, br, 2H, −NH); ^{13}C NMR (400 MHz, $CDCl_3$): δ = 190.0, 164.8, 155.8, 148.5, 142.2, 139.3, 134.9, 134.5, 134.1, 131.4, 128.5, 128.1, 126.8, 122.6, 120.9, 120.5, 117.7, 38.0, 24.7, 14.1 ppm; ESI mass in $CHCl_3$ calcd for $C_{61}H_{52}N_4O_3$, 889.09; found: *m*/*z* (%): 889.5 [M^+] (100), 890.5 [M^+] (70), 891.5 [M^+] (22).

***N*-Boc-[{2-amino}2,2′-(ethylenedioxy)]diethylamine (3a)**: This compound was prepared according to Muller et al.[34] A solution of di-*tert*-butyl bicarbonate (7.5 g, 0.034 mol) dissolved in dry $CHCl_3$ (100 mL) was added to a solution of 2,2′-(ethylenedioxy)diethylamine (50 mL, 0.34 mol) in $CHCl_3$ (300 mL) in 2.5 h with stirring in an ice-bath. The reaction was then allowed to stir for another 24 h at room temperature. It was then washed with water, extracted with $CHCl_3$ and dried over anhydrous Na_2SO_4. Solvent was the evaporated and the organic layer yielded the desired compound as pale yellow oil. Yield: 1.68 g, 20%; ^{1}H NMR ($CHCl_3$-d): δ = 5.2 (s, br, 1H, −NH), 3.64 (d, 4H), 3.5 (m, 4H), 3.3 (m, 2H), 2.85

(m, 2H), 1.6–1.4 ppm (m, 9H, Boc-H); ESI mass in $CHCl_3$ calcd for $C_{11}H_{24}N_2O_4$, 248.32; found: m/z (%): 249.0 [M^+] (100), 250 [M^+] (15), 149 [M^+, reactant amine] (35).

Benzyl-*N*-[{2-(*N*-Boc)}2,2′-(ethylenedioxy)diethylamino]glycinate (3b): This compound was prepared according to Kordatos et al.[35] A solution of benzyl 2-bromoacetate (0.64 mL, 4.02 mmol) in 1,4-dioxane (20 mL) was added slowly over a period of 1 h to a solution of **3a** (3 g, 0.012 mol) in 1,4-dioxane (20 mL) cooled at 0 °C. The reaction mixture was then stirred, overnight. The solvent was then evaporated under reduced pressure and the residue was dissolved in water and extracted with ethyl acetate. The organic extract was dried over anhydrous Na_2SO_4 and the solvent was evaporated under reduced pressure. The crude compound was purified by column chromatography on silica gel by using petroleum ether/ethyl acetate (70:30 to 50:50 v/v). Evaporation of the solvent yielded the desired product. Yield: 1.19 g, 75 %; ^{1}H NMR ($CHCl_3$-d): $\delta = 7.42$–7.39 (m, 5H, phenyl H), 5.22 (s, br, 1H, −NH), 5.18 (s, 2H), 3.6–3.51 (m, 6H), 3.5–3.46 (m, 4H), 3.28 (m, 2H), 2.8 (t, 2H), 1.45 ppm (s, 9H, Boc-H); ^{13}C NMR (400 MHz, CD_3OD): $\delta = 180.0$, 155.2, 79.0, 70.3, 69.9, 53.4, 49.3, 40.7, 27.4 ppm; ESI mass in $CHCl_3$ calcd for $C_{20}H_{32}N_2O_6$, 396.48; found: m/z (%): 397.1 [M^+] (18).

***N*-[2-(*N*-Boc)2,2′-(ethylenedioxy)diethylamino]glycine (3)**: Pd/C (80 mg, 5 %) was added to a methanolic solution of **3b** (1.25 g, 3.15 mmol), and the reaction mixture was stirred under hydrogen atmosphere for 24 h. The catalyst was then removed by filtration by using Celite and solvent was evaporated. The residue was triturated in diethyl ether to give the desired product as a white solid. Yield: 0.77 g, 80 %; ^{1}H NMR ($CHCl_3$-d): $\delta = 3.8$ (t, 2H), 3.7–3.55 (m, 8H), 3.5 (t, 2H), 1.40 ppm (s, 9H, Boc-H); ESI mass in H_2O calcd for $N_{13}H_{26}N_2O_6$, 306.36; found: m/z (%): 306.4 [M^-] (55), 305.5 [M^-] (40), 307.3 [M^-] (33).

Covalent functionalization of SWCNT(7,6) and SWCNT(6,5) with porphyrins (4): The synthesis of covalently functionalized carbon nanotube was carried out by 1,3-dipolar cycloaddition via azomethine ylide formation.[36–38] In a typical experiment, pristine SWCNT(7,6) (40 mg) was taken in DMF (40 mL) and the mixture was sonicated for 15 min by using a Mesonix ultrasonicator at 4 W power output. To the dispersed carbon nanotube/DMF solution were added porphyrin aldehyde **2** (10 mg) and Boc protected amino acid **3** (40 mg) and the reaction mixture was heated at 120 °C. After 24 h, porphyrin aldehyde **2** (10 mg) and Boc protected amino acid **6** (40 mg) were again added to the reaction flask. Another lot of the same amount was again added after 48 h and the reaction mixture was heated for 4 days in total. After being cooled to room temperature, the solution was filtered on a Millipore nylon membrane filter (0.2 μm). The black nanotube on the filter was washed with DMF, CH_2CH_2, MeOH. The residue was time and again sonicated, centrifuged and filtered until all the unreacted components were washed away. The final functionalized nanotube sample was then dried and used for further characterization by using UV/Vis/NIR, NIR fluorescence, Raman, TGA, TEM studies.

For the synthesis of covalently functionalized porphyrin–SWCNT(6,5), a similar procedure as above was followed. Finally, the H_2P–SWCNT hybrids (**4**) were converted to ZnP–SWCNT hybrids (**5**) by standard zinc-insertion reactions by using zinc acetate in methanol. The progress of the reaction was followed spectroscopically. After completion of the reaction, excess zinc acetate was removed by washing the reaction product with methanol.

ATR-IR analysis of functionalized nanohybrids: Peaks at 2800–3000 cm^{-1} corresponding to aliphatic C−H stretching, peaks in the range 3020–3100 cm^{-1} attributed to aromatic ring stretch, strong, broad hump at 1300–1600 cm^{-1} corresponding to phenyl ring stretch, peaks around 980–1050 cm^{-1} corresponding to C−O stretch, weak band at 3000–3200 cm^{-1} corresponding to N−H stretch, a peak at 1050 cm^{-1} due to C−N stretch, a band in the range 1600–1710 cm^{-1} attributed to carbonyl (C=O) stretch were observed in agreement with literature results.[39–40]

Preparation of nanocrystalline SnO_2 electrodes: These were prepared according to the literature procedure with few changes.[41] An SnO_2 colloidal solution (10 mL; Alfa Aesar, 15 %) was dissolved in ethanol (10 mL); NH_4OH (500 mL) was added to this solution for stability. About 0.5 mL of the colloidal solution was placed on an optically transparent electrode, fluorine doped indium tin oxide (FTO; Pilkington TEC-8, 6–9 Ω per square) and dried in air. The electrodes were annealed in an oven for 1 h in air at 673 K. The estimated thickness of the electrode was around 1–2 mm.

Instrumentation: The UV/Vis spectral measurements were carried out with a Shimadzu Model 2550 double monochromator UV/Vis spectrophotometer. The steady-state fluorescence spectra were measured by using a PerkinElmer (LS-55) and a Horiba Jobin Yvon Nanolog UV/Vis–NIR spectrofluorometer equipped with PMT (for UV/Vis) and InGaAs (for NIR) detectors. All the solutions were purged prior to spectral measurements by using Ar gas. ^{1}H and ^{13}C NMR spectra were obtained by using a Varian 400 MHz instrument. Tetramethylsilane ($Si(CH_3)_4$) was used as an internal standard.

Thermogravimetric analyses were run by using a Texas Instruments TGA Q50 instrument. All the samples for the analysis were dried under vacuum. Samples ramp test were performed under nitrogen atmosphere at 10 °C min^{-1}.

Transmission electron micrograph (TEM) measurements were recorded by applying a drop of the sample to a copper grid. Images were recorded on a Hitachi H7100 transmission electron microscope at an accelerating voltage of 100 kV for imaging.

The Raman spectra were measured by using Enwave Optronics, Inc., ProRaman-L instrument with 532 nm laser source. IR experiments were performed with a PerkinElmer Spectrum One FT-IR Spectrometer with universal ATR sampling accessory.

The time-resolved fluorescence spectra were measured by single photon counting method by using a streakscope (Hamamatsu Photonics, C5680) as a detector and the laser light (Hamamatsu Photonics M10306, laser diode head, 408 nm, pulse width = 71.5 ps) as an excitation source. Lifetimes were evaluated with software attached to the equipment.[40]

Nanosecond transient absorption measurements were carried out by using THG (532 nm) of a Nd:YAG laser (Spectra-Physics, Quanta-Ray GCR-130, 5 ns fwhm) as an excitation source. For transient absorption spectra in the near-IR region (600–1200 nm) and the time-profiles, monitoring light from a pulsed Xe lamp was detected with a Ge-APD (Hamamatsu Photonics, B2834). For the measurements in the visible region (400–1000 nm), a Si-PIN photodiode (Hamamatsu Photonics, S1722-02) was used as a detector.[42]

Photoelectrochemical experiments were performed in a two-electrode configuration by using desired donor–acceptor nanohybrids drop coated onto FTO/SnO_2 electrode and a platinized FTO electrode as counter electrode in acetonitrile solution containing LiI (0.5 M) and I_2 (0.1 M) as I^-/I_3^- redox mediator. The photocurrent–photovoltage characteristics of the solar cells were measured by using a Model 2400 Current/Voltage Source Meter of Keithley Instruments, Inc. (Cleveland, OH) under illumination with an AM 1.5 simulated light source with a Model 9600 of 150-W Solar Simulator of Newport Corp. (Irvine, CA).

Energy minimization calculations and the MO distributions and their energy levels by using B3LYP/3-21G(*) basis set of the nanohybrids were performed with Gaussian-09 software.[26] The frontier orbitals were generated by using the Gauss View program.

Acknowledgements

This work was financially supported by the National Science Foundation (Grant No. 1110942, to F.D.). A.S.D.S thanks Prof. H. Murata of JAIST for his kind support for this study.

[1] a) S. Iijima, *Nature* **1991**, *354*, 56–58; b) S. Iijima, T. Ichihashi, *Nature* **1993**, *363*, 603–605.

[2] a) P. J. F. Harris, *Carbon Nanotubes and Related Structures: New Materials for the Twenty-First Century*, Cambridge University Press, Cambridge, **2001**; b) *Carbon Nanotubes: Synthesis Structure and Ap-*

plications (Eds.: M. S. Dresselhaus, G. Dresselhaus, P. Avouris), Springer, New York, **2001**.

[3] a) *Handbook of Carbon Nano Materials, Vols. 1–4* (Eds.: F. D'Souza, K. M. Kadish), World Scientific, Singapore, **2011** and **2012**; b) S. Reich, C. Thomsen, J. Maultzsch, *Carbon Nanotubes: Basic Concepts and Physical Properties*, Wiley-VCH, Weinheim, **2004**; c) S. Roth, D. Carroll, *One-Dimensional Metals: Conjugated Polymers, Organic Crystals, Carbon Nanotubes*, Wiley-VCH, Weinheim, **2004**; d) M. Meyyappan, *Carbon Nanotubes, Science and Application*, Wiley-VCH, Weinheim, **2006**; e) R. Saito, G. Dresselhaus, M. D. Dresselhaus, *Physical Properties of Carbon Nanotubes*, Imperial College Press, London, **1998**.

[4] a) C. Staii, M. Chen, A. Gelperin, A. T. Johnson, *Nano Lett.* **2005**, *5*, 1774–1778; b) E. S. Jeng, A. E. Moll, A. C. Roy, J. B. Gastala, M. S. Strano, *Nano Lett.* **2006**, *6*, 371–375.

[5] a) M. Zheng, A. Jagota, E. D. Semke, B. A. Diner, R. S. McLean, S. R. Lustig, R. E. Richardson, N. G. Tassi, *Nat. Mater.* **2003**, *2*, 338–342; b) M. Zheng, A. Jagota, M. S. Strano, A. P. Santos, P. Barone, S. G. Chou, B. A. Diner, M. S. Dresselhaus, R. S. McLean, G. B. Onoa, G. G. Samsonidze, E. D. Semke, M. Usrey, D. J. Walls, *Science* **2003**, *302*, 1545–1548.

[6] a) S. Meng, P. Maragakis, C. Papaloukas, E. Kaxiras, *Nano Lett.* **2007**, *7*, 45–50.

[7] a) V. Sgobba, G. M. A. Rahman, D. M. Guldi, in *Carbon Nanotubes in Electron Donor–Acceptor Nanocomposites, Chemistry of Carbon Nanotubes* (Ed.: V. A. Basiuk), American Scientific, USA, **2006**; b) V. Sgobba, G. M. A. Rahman, C. Ehli, D. M. Guldi, in *Fullerenes-Principles and Applications* (Eds.: F. Langa, J. F. Nierengarten), Royal Society of Chemistry, Cambridge, **2007**; c) V. Sgobba, D. M. Guldi, *Chem. Soc. Rev.* **2009**, *38*, 165–184.

[8] a) J. L. Delgado, M. Á. Herranz, N. J. Martín, *Mater. Chem.* **2008**, *18*, 1417–1426; b) G. Bottari, G. de La Torre, D. M. Guldi, T. Torres, *Chem. Rev.* **2010**, *110*, 6768–3816; c) D. Tasis, N. Tagmatarchis, A. Bianco, M. Prato, *Chem. Rev.* **2006**, *106*, 1105–1136.

[9] S. Fukuzumi, T. Kojima, *J. Mater. Chem.* **2008**, *18*, 1427–1439.

[10] a) F. D'Souza, O. Ito, *Chem. Soc. Rev.* **2012**, *41*, 86–96; b) F. D'Souza, O. Ito, in *Handbook of Porphyrin Science, Vol. 1* (Eds.: K. M. Kadish, R. Guilard, K. M. Smith), World Science Publishers, Singapore, **2010**, pp. 307–437; c) F. D'Souza, O. Ito, *Chem. Commun.* **2009**, 4913–4928; d) F. D'Souza, A. S. D. Sandanayaka, O. Ito, *J. Phys. Chem. Lett.* **2010**, *1*, 2586–2590.

[11] a) S. M. Bachilo, L. Balzani, J. E. Herrara, F. Pompeo, D. E. Resasco, R. B. Weisman, *J. Am. Chem. Soc.* **2003**, *125*, 11186–11187; b) R. B. Weisman, S. M. Bachilo, *Nano Lett.* **2003**, *3*, 1235–1238; c) Z. Luo, L. D. Pfefferle, G. L. Haller, F. Papadimitrakopoulos, *J. Am. Chem. Soc.* **2006**, *128*, 15511–15516; d) S. Ghosh, S. M. Bachilo, R. B. Weisman, *Nat. Nanotechnol.* **2010**, *5*, 443–450; e) J.-D. R. Rocha, S. M. Bachilo, S. Ghosh, S. Arepalli, R. B. Weisman, *Anal. Chem.* **2011**, *83*, 7431–7437.

[12] a) Y. Tanaka, Y. Hirana, Y. Niidome, K. Kato, S. Saito, N. Nakashima, *Angew. Chem.* **2009**, *121*, 7791–7795; *Angew. Chem. Int. Ed.* **2009**, *48*, 7655–7659; b) L. Kavan, L. Dunsch, *Electrochemistry of Carbon Nanotubes in Carbon Nanotubes: Advanced Topics in the Synthesis Structure, Properties and Applications, Vol. III*, Springer, Berlin, **2008**; c) D. Paolucci, M. M. Franco, M. Iurlo, M. Marcaccio, M. Prato, F. Zerbetto, A. Penicaud, F. Paolucci, *J. Am. Chem. Soc.* **2008**, *130*, 7393–7399; d) C. Ehli, C. Oelsner, D. M. Guldi, A. Mateo-Alonso, M. Prato, C. Schmidt, C. Backes, F. Hauke, A. Hirsch, *Nat. Chem.* **2009**, *1*, 243–249.

[13] a) R. Krupe, F. Hennrich, *Adv. Eng. Mater.* **2005**, *7*, 111–116; b) M. C. Hersam, *Nat. Nanotechnol.* **2008**, *3*, 387–394; c) C. N. R. Rao, R. Voggu, A. Govindaraj, *Nanoscale* **2009**, *1*, 96–105; d) H. Zhang, B. Wu, W. Hu, Y. Liu, *Chem. Soc. Rev.* **2011**, *40*, 1324–1336.

[14] a) J. E. Herrera, D. E. Resasco, *Chem. Phys. Lett.* **2003**, *376*, 302–309; b) J. E. Herrera, B. F. Pompeo, D. E. Resasco, *J. Nanosci. Nanotechnol.* **2003**, *3*, 133–138; c) A. Jorio, A. P. Santos, H. B. Ribeiro, C. Fantini, M. Souza, J. P. M. Vieira, C. A. Furtado, J. Jiang, R. Saito, L. Balzano, D. E. Resasco, M. A. Pimenta, *Phys. Rev. B* **2005**, *72*, 075207/1–075207/5; d) F. Hennrich, R. Krupke, S. Lebedkin, K. Arnold, R. Fischer, D. E. Resasco, M. M. Kappes, *J. Phys. Chem. B* **2005**, *109*, 10567–10573.

[15] Also see the manufacturer's website: http://swentnano.com/ for additional product details.

[16] a) E. Maligaspe, A. S. D. Sandanayaka, T. Hasobe, O. Ito, F. D'Souza, *J. Am. Chem. Soc.* **2010**, *132*, 8158–8164; b) A. S. D. Sandanayaka, E. Maligaspe, T. Hasobe, O. Ito, F. D'Souza, *Chem. Commun.* **2010**, *46*, 8749–8751; c) A. S. D. Sandanayaka, N. K. Subbaiyan, S. K. Das, R. Chitta, E. Maligaspe, T. Hasobe, O. Ito, F. D'Souza, *ChemPhysChem* **2011**, *12*, 2266–2273; d) S. K. Das, N. K. Subbaiyan, F. D'Souza, A. S. D. Sandanayaka, T. Wakahara, O. Ito, *J. Porphyrins Phthalocyanines* **2011**, *15*, 1033–1043; e) S. K. Das, N. K. Subbaiyan, F. D'Souza, A. S. D. Sandanayaka, T. Hasobe, O. Ito, *Energy Environ. Sci.* **2011**, *4*, 707–716; f) F. D'Souza, S. K. Das, A. S. D. Sandanayaka, N. K. Subbaiyan, D. R. Gollapalli, M. E. Zandler, T. Wakahara, O. Ito, *Chem. Phys. Phys. Chem.* **2012**, *14*, 2940–2950.

[17] F. D'Souza, S. K. Das, M. E. Zandler, A. S. D. Sandanayaka, O. Ito, *J. Am. Chem. Soc.* **2011**, *133*, 19922–19930.

[18] *The Porphyrin Handbook, Vol. 9* (Eds.: K. M. Kadish, K. M. Smith, R. Guilard, Academic Press, San Diego, **2000**.

[19] M. A. Herrero, E. Vazquez, M. Prato, in *Handbook of Carbon Nano Materials, Vols. 1* (Eds.: F. D'Souza, K. M. Kadish), World Scientific, Singapore, **2011**, pp. 271–323.

[20] a) S. M. Bachilo, *Science* **2002**, *298*, 2361–2366; b) M. J. O'Connell, *Science* **2002**, *297*, 593–596; c) A. M. Rao, *Science* **1997**, *275*, 187–191; d) G. Gabriel, G. Sauthier, J. Fraxedas, M. Moreno-Manas, M. T. Martınez, C. Miravitlles, J. Casabo, *Carbon* **2006**, *44*, 1891–1897; e) J. Chen, M. A. Hamon, H. Hu, Y. Chen, A. M. Rao, P. C. Eklund, R. C. Haddon, *Science* **1998**, *282*, 95–98.

[21] a) E. P. Dillon, C. A. Crouse, A. R. Barron, *ACS Nano* **2008**, *2*, 156–164; b) I. W. Chiang, B. E. Brinson, A. Y. Huang, P. A. Willis, M. J. Bronikowski, J. L. Margrave, R. E. Smalley, R. H. Hauge, *J. Phys. Chem. B* **2001**, *105*, 8297–8301; c) J. D. Saxby, S. P. Chatfield, A. J. Palmisano, A. M. Vassallo, M. A. Wilson, L. S. K. Pang, *J. Phys. Chem.* **1992**, *96*, 17–18; d) S. Liu, X. Tang, Y. Mastai, I. Felner, A. Gedanken, *J. Mater. Chem.* **2000**, *10*, 2502–2506; e) F. E. Pinkerton, B. G. Wicke, C. H. Olk, G. G. Tibbetts, G. P. Meisner, M. S. Meyer, J. F. Herbst, *J. Phys. Chem. B* **2000**, *104*, 9460–9467.

[22] a) D. Baskaran, J. W. Mays, X. P. Zhang, M. S. Bratcher, *J. Am. Chem. Soc.* **2005**, *127*, 6916–6917; b) C. Ehli, S. Campidelli, F. G. Brunette, M. Prato, D. M. Guldi, *J. Porphyrins Phthalocyanines* **2007**, *11*, 442–447; c) K. H. Le Ho, L. Rivier, B. Jousselme, P. Jegou, A. Filoramo, S. Campidelli, *Chem. Commun.* **2010**, *46*, 8731–8733; d) T. Arai, S. Nobukuni, A. S. D. Sandanayaka, O. Ito, *J. Phys. Chem. C* **2009**, *113*, 14493–14499.

[23] a) F. Cordella, M. De Nardi, E. Menna, C. Hebert, M. A. Loi, *Carbon* **2009**, *47*, 1264–1269; b) B. Ballesteros, G. de La Torre, C. Ehli, G. M. Rahman, F. Agullo-Rueda, D. M. Guldi, T. Torres, *J. Am. Chem. Soc.* **2007**, *129*, 5061–5068.

[24] a) H. Ozawa, X. Yi, T. Fujigaya, Y. Nidome, T. Asano, N. Nakashima, *J. Am. Chem. Soc.* **2011**, *133*, 14771–14777; b) F. Cheng, J. Zhu, A. Adronov, *Chem. Mater.* **2011**, *23*, 3188–3194; c) P. Anilkumar, K. A. S. Fernando, L. Cao, F. Lu, F. Yang, W. Song, S. Sahu, H. Qian, T. J. Thorne, A. Anderson, Y-P. Sun, *J. Phys. Chem. C.* **2011**, *115*, 11010–11015; d) G. Bottari, J. A. Suanzes, O. Trukhina, T. Torres, *J. Phys. Chem. Lett.* **2011**, *2*, 905–913; e) J. Bartelmess, B. Ballesteros, G. de La Torre, D. Kiessling, S. Campidelli, M. Prato, T. Torres, D. M. Guldi, *J. Am. Chem. Soc.* **2010**, *132*, 16202–16211; f) W. C. Hung, G. Elias, C. M. Wai, *ChemPhysChem* **2010**, *11*, 3439–3446; g) J. Bartelmess, A. R. M. Soares, M. V. Martinez-Diaz, M. G. P. M. S. Neves, A. C. Tome, J. A. S. Cavaleiro, T. Torres, D. M. Guldi, *Chem. Commun.* **2011**, *47*, 3490–3492.

[25] a) Z. Zhang, Y. Che, R. A. Smaldone, M. Xu, B. R. Bunes, J. S. Moore, L. Zang, *J. Am. Chem. Soc.* **2010**, *132*, 14113–14117; b) U. Hahn, S. Engmann, C. Oelsner, C. Ehli, D. M. Guldi, T. Torres, *J. Am. Chem. Soc.* **2010**, *132*, 6392–6401; c) M. A. Herranz, C. Ehli, S. Campidelli, M. Gutierrez, G. L. Hug, K. Ohkubo, S. Fukuzumi, M. Prato, N. Martin, D. M. Guldi, *J. Am. Chem. Soc.* **2008**, *130*, 66–73;

d) J. S. Kavakka, S. Heikkinen, I. Kilpelainen, M. Mattila, H. Lipsanen, J. Helaja, *Chem. Commun.* **2007**, 519–521; e) P. J. Boul, D. G. Cho, G. M. A. Rahman, M. Marquez, Z. Lu, K. M. Kadish, D. M. Guldi, J. L. Sessler, *J. Am. Chem. Soc.* **2007**, *129*, 5683–5687; f) S. Y. Ju, F. Papadimitrakopoulos, *J. Am. Chem. Soc.* **2008**, *130*, 655–664; g) K. Saito, V. Troiani, H. Qui, N. Solladie, T. Sakata, H. Mori, M. Ohama, S. Fukuzumi, *J. Phys. Chem. C* **2007**, *111*, 1194–1199.

[26] Gaussian 09, M. J. Frisch, G. W. Trucks, H. B. Schlegel, G. E. Scuseria, M. A. Robb, J. R. Cheeseman, V. G. Zakrzewski, J. A. Montgomery, R. E. Stratmann, J. C. Burant, S. Dapprich, J. M. Millam, A. D. Daniels, K. N. Kudin, M. C. Strain, O. Farkas, J. Tomasi, V. Barone, M. Cossi, R. Cammi, B. Mennucci, C. Pomelli, C. Adamo, S. Clifford, J. Ochterski et al., Gaussian, Inc., Pittsburgh PA, **2009**.

[27] K. M. Kadish, *Prog. Inorg. Chem.* **1986**, *34*, 435–605.

[28] a) D. Rehm, A. Weller, *Isr. J. Chem.* **1970**, *10*, 259–171; b) N. Mataga, H. Miyasaka, in *Electron Transfer* (Eds.: J. Jortner, M. Bixon), Wiley, New York, **1999**, pp. 431–496.

[29] J. R. Lakowicz, *Principles of Fluorescence Spectroscopy*, 3rd ed., Springer, New York, **2006**.

[30] N. J. Turro, V. Ramamurty, J. C. Scaiano, *Priciples of Molecular Photochemistry, An Introduction*, University Science Book, California, **2009**.

[31] a) *Dye-Sensitized Solar Cells* (Ed.: K. Kalyanasundaram), EPFL Press, Lausanne, **2010**; b) B. C. O'Regan, M. Grätzel, *Nature* **1991**, *353*, 737–740; c) P. V. Kamat, *J. Phys. Chem. C* **2007**, *111*, 834–2860; d) T. Umeyama, H. Imahori, *Energy Environ. Sci.* **2008**, *1*, 120–133; e) T. Hasobe, *Phys. Chem. Chem. Phys.* **2010**, *12*, 44–57; f) N. K. Subbaiyan, C. A. Wijesinghe, F. D'Souza, *J. Am. Chem. Soc.* **2009**, *131*, 14646–14647.

[32] IPCE $[\%] = 100 \times 1240 \times I_{SC}/(W_{in} \times \lambda)$, where I_{SC} is the short circuit photocurrent $[A\,cm^{-2}]$, W_{in} is the incident light intensity $[W\,cm^{-2}]$, and λ is the wavelength [nm].

[33] A. D. Adler, R. F. Longo, J. D. Finarelli, J. Goldmacher, J. Assour, L. Korsakoff, *J. Org. Chem.* **1967**, *32*, 476.

[34] D. Muller, I. Zeltser, G. Bitan, C. Gilon, *J. Org. Chem.* **1997**, *62*, 411–416.

[35] K. Kordatos, T. Da Ros, S. Bosi, E. Vazquez, M. Bergamin, C. Cusan, F. Pellarini, V. Tomberli, B. Baiti, D. Pantarotto, V. Georgakilas, G. Spalluto, M. Prato, *J. Org. Chem.* **2001**, *66*, 4915–4920.

[36] M. Maggini, G. Scorrano, M. Prato, *J. Am. Chem. Soc.* **1993**, *115*, 9798–9799.

[37] V. Georgakilas, K. Kordatos, M. Prato. D. M. Guldi, M. Holzinger, A. Hirsch, *J. Am. Chem. Soc.* **2002**, *124*, 760–761.

[38] V. Georgakilas, N. Tagmatarchis, D. Pantarotto, A. Bianco, J-P. Briand, M. Prato, *Chem. Commun.* **2002**, 3050–3051.

[39] A. Mukherjee, R. Combs, J. Chattopadhyay, D. W. Abmayr, P. S. Engel, W. E. Billups, *Chem. Mater.* **2008**, *20*, 7339–7343.

[40] J. Zhu, J. D. Kim, H. Peng, J. L. Margrave, V. N. Khabashesku, E. V. Barrera, *Nano Lett.* **2003**, *3*, 1107–1113.

[41] a) I. Bedja, S. Hotchandani, R. Carpentieer, R. Fessenden, P. V. Kamat, *J. Appl. Phys.* **1994**, *75*, 5444–5447; b) N. K. Subbaiyan, E. Maligaspe, F. D'Souza, *ACS Appl. Mater. Interfaces* **2011**, *3*, 2368–2376.

[42] A. S. D. Sandanayaka, R. Chitta, N. K. Subbaiyan, L. D'Souza, O. Ito, F. D'Souza, *J. Phys. Chem. C* **2009**, *113*, 13425–13432.

Received: March 21, 2012
Published online: ■■ ■■, 0000

Photoelectrochemistry

S. K. Das, A. S. D. Sandanayaka, N. K. Subbaiyan, M. E. Zandler, O. Ito, F. D'Souza** ..... ▮▮▮▮–▮▮▮▮

Functionalization of Diameter Sorted Semi-conductive SWCNTs with Photosensitizing Porphyrins: Syntheses and Photoinduced Electron Transfer

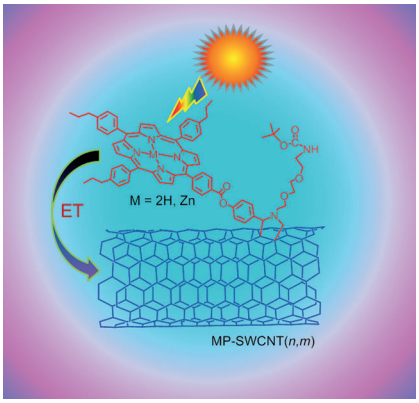

Size matters! Diameter dependent efficiencies of photoinduced electron transfer leading to charge stabilization, and photoelectrochemical response of solar cells is demonstrated in porphyrin covalently linked to (7,6) and (6,5) enriched single wall carbon nanotube donor–acceptor nanohybrids (see figure).